*J. Fluid Mech.* (1994), *vol.* 280, *pp.* 227–253



# Nonlinear compressible magnetoconvection Part 2. Streaming instabilities in two dimensions

By M. R. E. PROCTOR, N. O. WEISS, D. P. BROWNJOHN AND N. E. HURLBURT†

Department of Applied Mathematics and Theoretical Physics, University of Cambridge, Silver Street, Cambridge CB3 9EW, UK

(Received 3 August 1993 and in revised form 15 June 1994)

We have conducted further numerical experiments on two-dimensional fully compressible convection in an imposed vertical magnetic field and interpreted the results by reference to appropriate low-order models. Here we focus on streaming instabilities, involving horizontal shear flows, which form an important mechanism for the breakdown of steady convection in relatively weak fields for boxes of sufficiently small aspect ratio. While these shearing modes can arise even in the absence of a field, they will typically lead only to travelling and modulated waves unless there is a field to provide a restoring force. For magnetoconvection a new and dramatic form of pulsating wave appears after a complex sequence of secondary bifurcations.

## 1. Introduction

Fluid mechanics provides many examples where small-scale motion gives rise to large-scale streaming flows. This process has been demonstrated experimentally for turbulent convection in an annular container (Krishnamurti & Howard 1981) and has been explored theoretically in a wide range of contexts. The underlying mechanism is straightforward. Consider two-dimensional motion in a fluid layer with rolls corresponding to a row of vortex tubes of alternating sign: if the rolls tilt they will transport horizontal momentum towards the boundaries of the layer, generating a sheared flow that enhances the tilt (Howard & Krishnamurti 1986). Thus there is a potential instability, leading to solutions whose form depends upon the details of the system. These streaming instabilities occur frequently in numerical studies of compressible convection. As an illustration, we show some results for fully compressible two-dimensional convection, driven by internal heating in a strongly stratified layer with periodic lateral boundary conditions. The streaklines in figure 1(*a*) correspond to a mildly nonlinear steady solution which is stable. The pattern is mirror-symmetric about vertical planes centred on the rising and falling plumes but there is no up-down symmetry in the system. The mirror-symmetry is broken in a bifurcation that gives rise to a pair of travelling waves; figure 1(*b*) shows a rightward travelling wave, in the frame with no net horizontal momentum. The horizontally averaged velocity represents a sheared flow with vorticity corresponding to a clockwise sense of motion. As a result, one roll is boosted while the other is almost suppressed. Similar behaviour is found in Boussinesq convection too. For the standard Rayleigh–Bénard problem, rolls retain point-symmetry about their centres and so the pattern cannot travel. Thus the

† Permanent address: Lockheed Palo Alto Research Laboratories, Palo Alto, CA 94304, USA.

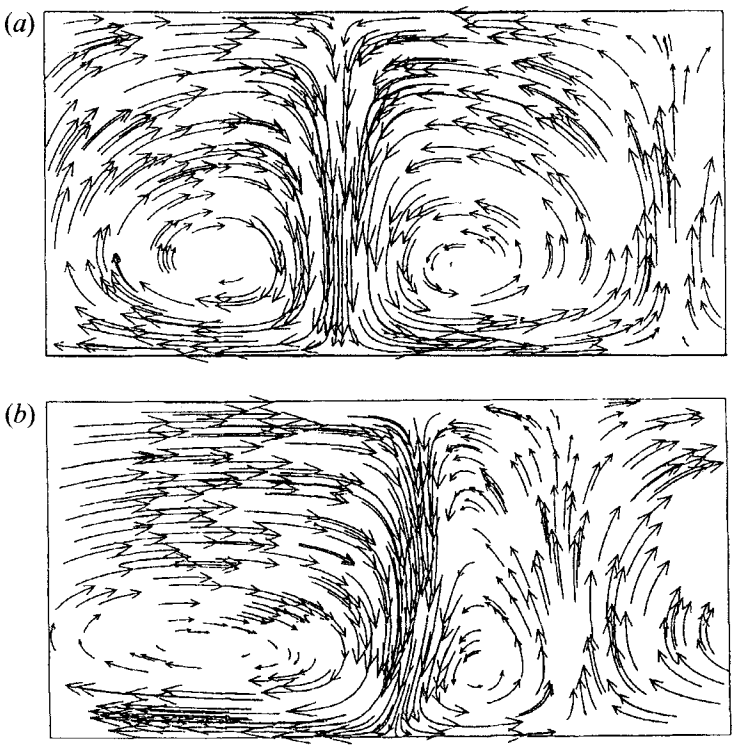


FIGURE 1. Symmetry-breaking and streaming instabilities. Streaklines for compressible convection driven by internal heating. (*a*) Steady convection: the solution possesses mirror symmetry about vertical planes. (*b*) A rightward travelling wave: the symmetry is broken and there is a net shear in the velocity.

analogue of the travelling wave is steady tilted convection, with a mean streaming motion that enhances each alternate roll (Howard & Krishnamurti 1986; Proctor & Weiss 1993; Matthews *et al.* 1993).

Travelling waves, like steady tilted convection, arise from a stationary (pitchfork) bifurcation. The mirror-symmetry of the original steady solution may also be broken in an oscillatory (Hopf) bifurcation, giving rise to *pulsating waves* (Landsberg & Knobloch 1991; Proctor & Weiss 1993). These waves are periodic and possess a symmetry such that advancing the solution half a period in time is equivalent to reflection about the original mirror-planes. This spatiotemporal symmetry ensures that there is no net drift over a full period of the oscillation. Pulsating waves have also been described as 'direction-reversing travelling waves' (Landsberg & Knobloch 1991) or, more straightforwardly, as 'sloshing' (Lantz & Sudan 1994; Lantz 1994). Breaking their spatiotemporal symmetry gives rise to modulated waves, which are periodic in a uniformly moving frame. Conversely, travelling waves may undergo an oscillatory bifurcation that gives rise to modulated waves, which may themselves develop into pulsating waves after a further global bifurcation (Matthews *et al.* 1993).

There has been a recent surge of interest in streaming instabilities – together with the development of travelling waves, modulated waves, pulsating waves and yet more complicated time-dependent behaviour – in a variety of contexts. Ordinary Boussinesq convection has been investigated with ever-increasing precision (Deardorff & Willis 1965; Howard & Krishnamurti 1986; Finn 1993; Prat, Massaguer & Mercader 1993; Julien, Brummell & Hart 1994). Studies of compressible convection, with an

astrophysical motivation, have also revealed complicated shearing motions (Hurlburt, Toomre & Massaguer 1984; Ginet & Sudan 1987). Since shear flows suppress convective transport the streaming instability might be exploited to reduce heat losses in plasma devices such as tokamaks (Drake *et al.* 1992; Finn, Drake & Guzdar 1992). Modulated waves appear in Taylor–Couette flow (Coughlin & Marcus 1992*a*, *b*) as well as for convection in a rotating system (Schnaubelt & Busse 1992). So the development of streaming motion should be significant both for meteorology and for the study of planetary atmospheres.

Compressible magnetoconvection provides the cleanest demonstration of transitions between steady convection, travelling waves, modulated waves, pulsating waves and chaotic oscillations. If mirror symmetry is imposed by adopting fixed lateral boundaries, as in earlier Boussinesq investigations (Weiss 1981; Proctor & Weiss 1982), then stable steady solutions can be found. However, such solutions are likely to become unstable if the boundary conditions are relaxed. In this paper we describe the development of these streaming instabilities; in contrast to previous work, we adopt horizontally periodic boundary conditions and consider a fully compressible fluid layer.

The original motivation for studying this problem was to understand convection in sunspot umbrae, which are permeated by a strong vertical magnetic field (Thomas & Weiss 1992). The great majority of work undertaken has assumed two-dimensional flows and fields (see the reviews by Hughes & Proctor 1988; Weiss 1991; Proctor 1992), although some three-dimensional computations have been completed recently (Matthews 1993; Matthews, Proctor & Weiss 1994*b*). Such idealized investigations are an essential counterpoint to other, more observationally oriented numerical simulations (e.g. Nordlund & Stein 1990; Grossmann-Doerth *et al.* 1994). Hurlburt *et al.* (1989, hereinafter referred to as Part 1) considered a relatively shallow layer, in order to isolate the interaction of compressibility and strong magnetic fields. As in the equivalent Boussinesq problem, where the density and properties of the layer are essentially independent of depth, the initial bifurcation to convection from the trivial state can be oscillatory when the imposed magnetic field is sufficiently strong (for a review of the Boussinesq problem see Proctor & Weiss 1982). In Part 1 the resulting oscillatory motion was studied in the fully nonlinear regime; Weiss *et al.* (1990) have also investigated both steady and oscillatory convection in much deeper layers, with a view to understanding convection in the stratified umbra of a sunspot. The final paper in this series (Part 3) will be concerned with behaviour when the imposed field is horizontal; a similar configuration has been studied independently by Lantz & Sudan (1994) and Lantz (1994).

In the present paper we remain, as in Part 1, with a relatively shallow layer. First of all, we consider briefly the case when the field strength is just above the critical value for an initial oscillatory bifurcation to occur, and investigate the interactions between steady convection, travelling waves and standing waves at relatively low amplitudes. Then we focus on the situation in which the imposed field is much weaker, so that there is, typically, a stationary bifurcation from the static, conducting solution. Of particular interest is the question of how the steady convection rolls that arise at the primary bifurcation lose stability to time-dependent motion. This process depends on the aspect ratio of our computational domain. For wider boxes, resonant interactions between modes with different horizontal scales lead to travelling waves and modulated waves – as discussed for non-magnetic convection by Jones & Proctor (1987), Proctor & Jones (1988) and Julien (1991). Much more interesting is the scenario in narrower boxes, with fields that are much weaker than those considered in Part 1. Now we find

the frequent occurrence of a new type of periodic solution, involving vigorous oscillatory horizontal streaming motion (Weiss 1989). In these solutions the Lorentz force ensures that the sheared horizontal velocity reverses exactly after half a period, so they possess the spatiotemporal symmetry of pulsating waves. The transition from steady cellular convection to pulsating waves involves intermediate branches of travelling waves and modulated waves. Similar behaviour has been found for convection with a horizontal field, in the anelastic approximation (Lantz & Sudan 1994; Lantz 1994), and analogous transitions can also be identified in Boussinesq magnetoconvection (Rucklidge & Matthews 1993, 1994; Matthews *et al.* 1993). In the absence of a magnetic field such vigorous pulsating waves appear to be less common.

It is hard when conducting numerical experiments to be sure that one has captured all the different types of behaviour. Crucial sequences of transitions frequently appear over a very small range of parameters and, above all, it is impossible to observe unstable branches directly. To establish the bifurcation structure it is therefore essential to construct low-order systems of ordinary differential equations which reproduce the changes that are observed and can be studied in much greater detail. Such model systems can be obtained, for instance, from a severely truncated representation of the variables in the partial differential equations. In the case of pulsating waves an appropriate model is readily to hand. It turns out that such a simple system can indeed be constructed for the Boussinesq problem (Rucklidge & Matthews 1993, 1994; Matthews *et al.* 1993). While the differing symmetries of compressible and Boussinesq magnetoconvection do not allow a complete analogy, there is a correspondence between the two problems which allows the model to be used in a slightly adapted form that captures all the principal transitions.

The paper is organized as follows: in §2 we formulate the problem and summarize the results of linearized stability theory. Section 3 is concerned with behaviour at moderate field strengths, near the point of transition from an oscillatory to a stationary primary bifurcation; it also includes a brief discussion of drift phenomena in wide boxes, associated with coupling between two- and four-roll convection modes. Section 4 deals with narrower cells and presents our most important results. Here the streaming instabilities are prominent and pulsating waves appear in a dramatic form. The associated bifurcation sequence, involving branches of travelling waves and modulated waves, can also be established. This bifurcation structure is related to that for a low-order system of ordinary differential equations in §5. We conclude in §6 by connecting our results to very recent three-dimensional numerical experiments.

## 2. Linear stability

We consider two-dimensional magnetoconvection in a perfect monatomic gas, in the presence of an imposed vertical magnetic field. The model problem is identical with that discussed in Part 1. Motion in the region $\{0 \leqslant x \leqslant \lambda;\ z_0 \leqslant z \leqslant z_0+1\}$ is governed by the dimensionless equations

$$P = \rho T, \quad \frac{\partial \rho}{\partial t} = -\boldsymbol{\nabla}\cdot(\rho \boldsymbol{u}), \tag{2.1}$$

$$\boldsymbol{\nabla}\cdot\boldsymbol{B} = 0, \quad \frac{\partial \boldsymbol{B}}{\partial t} = \boldsymbol{\nabla}\times(\boldsymbol{u}\times\boldsymbol{B}) + \zeta_0 \bar{K}\nabla^2 \boldsymbol{B}, \tag{2.2}$$

$$\frac{\partial}{\partial t}(\rho \boldsymbol{u}) = -\boldsymbol{\nabla}\cdot(\rho \boldsymbol{u}\boldsymbol{u} - F\boldsymbol{B}\boldsymbol{B}) - \boldsymbol{\nabla}(P + \tfrac{1}{2}F|\boldsymbol{B}|^2) + (m+1)\rho\hat{\boldsymbol{z}} + \boldsymbol{\nabla}\cdot\boldsymbol{\tau} \tag{2.3}$$

and

$$\frac{\partial}{\partial t}\left[\rho\left\{\frac{T}{\gamma-1}+\tfrac{1}{2}|\boldsymbol{u}|^2-(m+1)z\right\}+\tfrac{1}{2}F|\boldsymbol{B}|^2\right]$$

$$=-\boldsymbol{\nabla}\cdot\left[\rho\left\{\frac{\gamma T}{\gamma-1}+\tfrac{1}{2}|\boldsymbol{u}|^2-(m+1)z\right\}\boldsymbol{u}+F\boldsymbol{B}\times(\boldsymbol{u}\times\boldsymbol{B}-\zeta_0\bar{K}\boldsymbol{\nabla}\times\boldsymbol{B})-\bar{K}\boldsymbol{\nabla}T-\boldsymbol{u}\cdot\boldsymbol{\tau}\right]. \quad (2.4)$$

Here $\bar{K}$ is a dimensionless thermal conductivity and $\zeta_0\bar{K}$ is the dimensionless magnetic diffusivity, while $\boldsymbol{\tau}$ is the stress tensor for a Newtonian fluid with constant shear viscosity $\mu$; the Prandtl number $\sigma=\mu c_p/K$ is thus uniform. The quantity $F$ was used in Part 1 as a measure of the field strength; in the present paper we use instead the 'plasma $\beta$', namely $\hat{\beta}\equiv 2(z_0+\frac{1}{2})^{m+1}/Fz_0^m$, a measure of the ratio between gas pressure and magnetic pressure. The other symbols have their usual meanings (see Part 1). We take this opportunity to correct an erroneous formulation of the equation of motion in Part 1 (the numerical scheme used in that paper is, however, correct), as well as transcription errors in equations (7) and (8) of Weiss *et al.* (1990). (These errors did not affect the computational results.)

We adopt the standard illustrative (free) boundary conditions at the top and bottom of the layer, together with periodic lateral boundary conditions. Thus $T=z_0, z_0+1$ at the upper and lower boundaries, respectively, while $u_z=\partial u_x/\partial z=B_x=0$. The conditions on the magnetic field aim to reproduce conditions at the top of the solar atmosphere while making minimal demands on knowledge of the conditions outside the layer. All quantities are assumed to be periodic in $x$ with period $\lambda$. For this paper we again take a static reference atmosphere with $z_0=\frac{1}{6}$ and a polytropic index $m=\frac{1}{4}$. While the density contrast between the top and bottom of this layer is a moderate 1.63, there is some variation of physical quantities with $z$. We use a circumflex to denote the value of a quantity at the middle of this layer ($z=\frac{2}{3}$). The ratio $\zeta$ of the magnetic to the thermal diffusivity is proportional to the density, so that $\hat{\zeta}=\sqrt{2}\zeta_0$. We set $\sigma=\hat{\zeta}=0.1$. Then the state of the system is fixed by specifying the aspect ratio $\lambda$, the Rayleigh number $\hat{R}$ and either the Chandrasekhar number $Q$ or the plasma beta $\hat{\beta}$, given by

$$\hat{R}=\frac{75}{4\bar{K}^2},\quad \hat{\beta}=\left(\frac{128}{9}\right)\frac{\hat{R}}{Q}. \quad (2.5)$$

We shall study behaviour in a parameter range where instability first sets in at a stationary bifurcation as $\hat{R}$ is increased. The bifurcation value $\hat{R}^{(e)}$ depends both on $\lambda$ and on $Q$ (or $\hat{\beta}$). Figure 2 shows $\hat{R}^{(e)}$ as a function of $Q$ for $\lambda=1$, 2 and 4 (the values used in this paper) calculated with a program developed by Cattaneo (1984). The values of $\hat{R}^{(e)}$ are only 10–15% higher than those for a Boussinesq fluid, since the layer is weakly stratified. The magnetic field has no influence if $Q\ll 1$ and in the Boussinesq limit convection then occurs first for $\lambda=2\sqrt{2}$, so it is not surprising that the values of $\hat{R}^{(e)}$ for $\lambda=2$, 4 are almost equal, with the latter slightly less, while $\hat{R}^{(e)}$ is significantly greater for $\lambda=1$. The values of $\hat{R}^{(e)}$ increase with increasing $Q$ and narrower cells are preferred when $Q$ is large. For $Q>300$, $\hat{R}^{(e)}$ is least for $\lambda=1$. When $Q\gg 1$ the bifurcation value $\hat{R}^{(e)}$ is approximately proportional to $Q$ and the bifurcation sets are therefore parallel to lines of constant $\hat{\beta}$, which are indicated in the figure. In this limit we find that the stationary bifurcations for $\lambda=1$, 2 and 4 occur near $\hat{\beta}=210$, 310 and 720, respectively.

If we restrict our attention to square rolls with $\lambda=2$, we can distinguish three

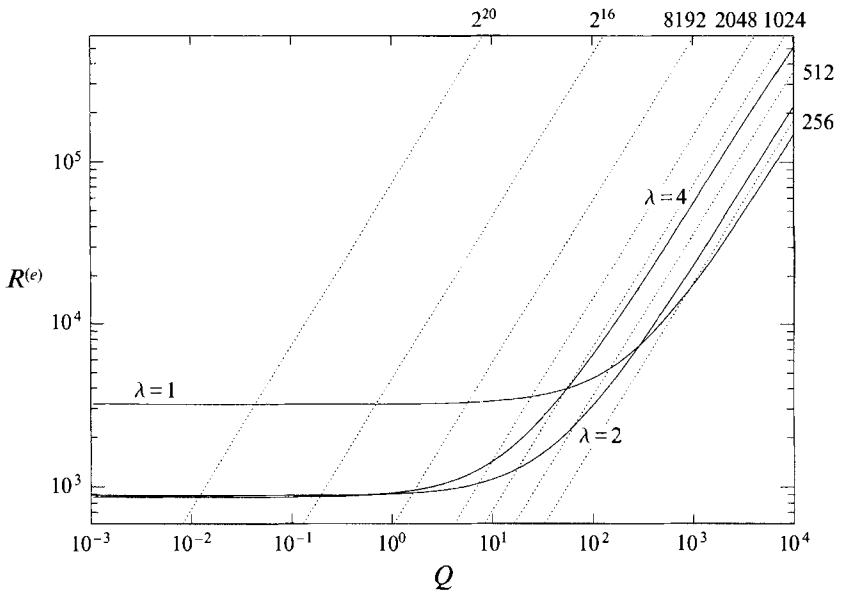


FIGURE 2. Linear stability: $R^{(e)}$ as a function of $Q$ for $\lambda = 1$, 2 and 4. $\sigma = \hat{\zeta} = 0.1$, $z_0 = \frac{1}{6}$. Values of $\hat{\beta}$ are indicated on the sloping lines, along which $\hat{\beta}$ is constant.

different regimes. In the absence of a magnetic field convection sets in at $\hat{R}^{(e)} = 890$, and $\hat{R}^{(e)} = 1000$ when $Q \approx 5$ ($\hat{\beta} \approx 2800$). Thus magnetic effects are only a small perturbation for $\hat{\beta} > 2048$. At the other extreme, for $Q > 50$ ($\hat{\beta} < 540$), the stationary bifurcation is preceded by an oscillatory bifurcation, giving rise to branches of standing wave and travelling wave solutions (cf. Part 1, figure 1). Thus the magnetic field is dominant for $\hat{\beta} < 512$. It is with the intermediate range, $512 \leqslant \hat{\beta} \leqslant 2048$, that this paper is mainly concerned.

The numerical experiments described here were carried out using the code described in Part 1, which relies on a two-step Lax–Wendroff scheme (Graham 1975; Hurlburt & Toomre 1988). For most of the runs sufficient accuracy was obtained with 40 mesh intervals in the $z$-direction. Some results have been confirmed using a more sophisticated code (Matthews *et al.* 1994*a*). A complete list of the runs carried out and reported on here is given in the Appendix.

As a dimensionless measure of convective efficiency in the nonlinear regime we use the normalized superadiabatic heat transport, given by the Nusselt number

$$N = 2F_T/\bar{K} - 1, \tag{2.6}$$

where $F_T$ is the total energy flux. In the absence of convection $N = 1$. An alternative measure is the spatially averaged kinetic energy density $\langle \frac{1}{2}\rho |\boldsymbol{u}|^2 \rangle$.

## 3. Steady convection, travelling waves and pulsating waves

In the majority of this section (except for §3.3) we describe nonlinear solutions obtained for $\lambda = 2$. In the weak field limit we expect to find steady convection in rolls with square cross-section (cf. Hurlburt *et al.* 1984). These steady solutions, like the standing waves that appear when the field is strong, possess mirror-symmetry about vertical planes with a spacing $\frac{1}{2}\lambda$ that separate the rolls. The mirror-symmetry of

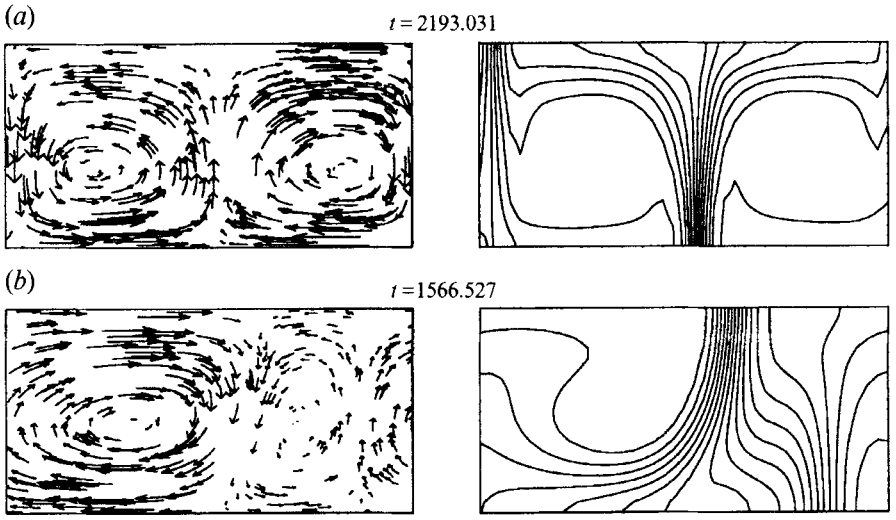


FIGURE 3. (*a*) Streaklines and field lines for a mirror-symmetric steady solution with $\lambda = 2$, $\hat{R} = 2000$ and $\hat{\beta} = 2048$. (*b*) The same, but for an asymmetric leftward travelling wave with $\hat{\beta} = 1024$.

a steady solution can be broken in a stationary bifurcation, which gives rise to branches of travelling wave solutions, or in an oscillatory bifurcation, which gives rise to pulsating waves, characterized by an alternating horizontal streaming flow and associated reversals of the direction of drift of the cells (Proctor & Weiss 1993). Subsequent bifurcations may lead to modulated waves. We provide examples of symmetry-breaking bifurcations in the intermediate-field regime that are followed by the appearance of travelling waves and of pulsating waves, and show how the former are related to standing waves and to the oscillatory bifurcation from the static (trivial) solution.

### 3.1. *Travelling waves and standing waves* ($\hat{R} = 2000$)

Convection sets in at a stationary (pitchfork) bifurcation when the field is weak and at an oscillatory (Hopf) bifurcation when the field is strong. At the transition there is a bifurcation of codimension two with a double-zero eigenvalue. For our choice of parameters this multiple (Takens–Bogdanov) bifurcation occurs when $\hat{\beta} = 540$ and $\hat{R} = 1900$. We begin by investigating weakly nonlinear behaviour. Thus we set $\hat{R} = 2000$ and study the effect of varying the magnetic field. It should be noted that the product of $Q$ and $\hat{\beta}$ is proportional to $\hat{R}$, so that for fixed $\hat{R}$ only one of these parameters may be independently varied.

In the strong-field regime there is a Hopf bifurcation at $\hat{\beta} = 32$, followed by a pitchfork bifurcation at $\hat{\beta} = 520$. At the other extreme, for $\hat{\beta} \gg 1$, we have $\hat{R} \approx 2.25\hat{R}^{(e)}$ and obtain steady convection with $N = 1.899$ and $\langle \frac{1}{2}\rho|\boldsymbol{u}|^2 \rangle = 0.196$. Though the layer is quite shallow, the effects of compressibility may be seen near the top of the layer, where the sound speed $v_s = (\gamma T)^{1/2}$ is least. At the top of the layer, although convection is weak, the density drops locally to 8% below its reference value of unity, while the Mach number $M = |\boldsymbol{u}|/v_s$ reaches a local maximum value of 1.15. As the imposed magnetic field is increased, stable steady solutions persist up to $\hat{\beta} = 2048$ ($Q = 13.89$); their amplitude is only slightly reduced, so that $N = 1.848$, $\langle \frac{1}{2}\rho|\boldsymbol{u}|^2 \rangle = 0.184$. Streak lines and field lines for this solution are illustrated in figure 3(*a*). There are vertical planes of symmetry near $x = 0$, 1 whose location is determined by initial conditions.

For $\hat{\beta} = 1024$ we find a transient steady solution with $N = 1.77$ which gives way to

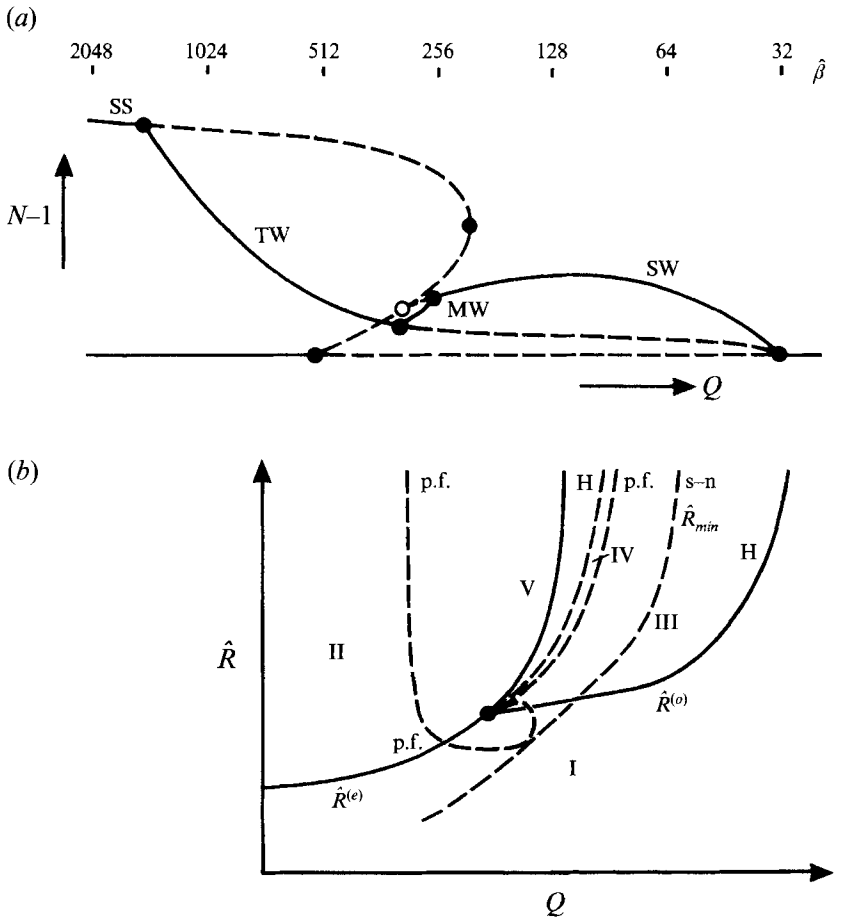


FIGURE 4. (*a*) Schematic bifurcation diagram, showing $(N-1)$ as a function of $Q$, for $\lambda = 2$, $\hat{R} = 2000$. As $Q$ decreases the trivial static solution undergoes a Hopf bifurcation followed by stable standing waves (SW), which give way to modulated waves (MW), travelling waves (TW) and finally to stable symmetric steady convection (SS). (*b*) Bifurcation structure in the $(Q,\hat{R})$-plane: the primary Hopf and pitchfork bifurcations are indicated by full lines and secondary bifurcations are denoted by broken lines. In region I the static state is stable; in region II there are stable steady solutions; SW are stable in region III, MW in region IV and TW in region V. Hopf, pitchfork and saddle-node bifurcations are denoted by H, p.f. and s-n respectively.

travelling waves. There is a substantial drop in heat transport to $N = 1.185$, with a corresponding fall in kinetic energy, and the waves propagate with a velocity $V = 0.0018$. Figure 3(*b*) shows the velocity and magnetic field for a leftward propagating wave. Note the loss of reflection symmetry and the predominance of the clockwise-rotating roll. At $\hat{\beta} = 512$ there is an unstable steady solution with $N = 1.57$, followed by stable travelling waves with $N = 1.15$ and $V = 0.0043$. Once again, the preferred solution is much less effective at transporting heat. For $\hat{\beta} = 256$, 128 there are stable standing wave solutions (periodic oscillations with reversals of the flow) with an amplitude that is very small. This is to be expected since we are close to the linear stability boundary (near $\hat{R} = 1900$) for these smallish values of $\hat{\beta}$.

These results allow us to construct the bifurcation diagram in figure 4(*a*). As $\hat{\beta}$ is increased for fixed $\hat{R}$ there is first a Hopf bifurcation at $\hat{\beta} = 32$ giving rise to stable standing waves and a pair of unstable travelling wave solutions. The branch of

standing wave solutions loses stability in a secondary pitchfork bifurcation around $\hat{\beta} = 300$, shedding a short branch of modulated waves which transfer stability to the travelling waves. Although the modulated waves have not been found numerically, they are necessary to effect the stability transfer, though the branch may be stable or unstable. This pattern is familiar from Part 1. The pitchfork bifurcation from the trivial solution at $\hat{\beta} = 520$ gives rise to unstable steady solutions on a branch that has a turning point (corresponding to a saddle-node bifurcation) around $\hat{\beta} = 200$. The branch of travelling wave solutions finally meets the steady branch, which acquires stability in a pitchfork bifurcation around $\hat{\beta} = 1500$. Figure 4(*b*) shows the corresponding bifurcation set in the $(Q, \hat{R})$-plane. This bifurcation structure is related to that found for thermosolutal convection (Moore & Weiss 1990) but differs from those obtained for the Takens–Bogdanov bifurcation with $O(2)$ symmetry by Dangelmayr & Knobloch (1987) owing to the presence of a saddle-node bifurcation on the steady branch. Without this additional turning point we would expect to recover the bifurcation structure found for narrow rolls with $\lambda = 1$ and illustrated in figure 11(*b*) of Part 1.

For $\hat{R} = 1750$ and $\hat{\beta} = 830$ ($Q = 30$), below the Takens–Bogdanov point in figure 4(*b*), we find a transient steady solution ($N = 1.6$) which gives way to stable travelling waves. Thus travelling wave solutions exist in a region of the $(\hat{\beta}, \hat{R})$-plane where linear theory suggests that only steady solutions should occur. The line of secondary pitchfork bifurcations emerges with a positive gradient from the Takens–Bogdanov point; at this stage the pitchfork bifurcation is on the lower branch of the steady-state curve. Later, however, as shown in figure 4(*a*) it lies on the upper portion, and so the line must touch the line of saddle-nodes for the steady branch. The simplest diagram compatible with the results is shown in figure 4(*b*). This complicated structure will be discussed in greater detail in Part 3, since it is also to be found for imposed horizontal fields.

### 3.2. *Steady convection and pulsating waves*

We now consider what happens for larger values of $\hat{R}$. The strong-field regime ($\hat{\beta} \leqslant 128$) investigated in Part 1 yielded solutions that are typically oscillatory. For weaker field ($\hat{\beta} \geqslant 2048$) steady solutions are recovered but the transition between these regions is marked by complicated spatiotemporal behaviour. For $\hat{\beta} = 256$ the low-amplitude standing waves found with $\hat{R} = 2000$ disappear when $\hat{R} = 4000$. Instead, there is a transient steady solution which is followed by aperiodic oscillations that lack reflection symmetry. Similar behaviour is found for $\hat{R} = 8000$ with $\hat{\beta} = 256$, 512 and 1024. These chaotic solutions seem to have developed from modulated waves but they share some features with the pulsating waves to be described below and in §5.

Stable steady convection rolls appear again in the weak-field regime, for $\hat{R} = 8000$ and $\hat{\beta} \geqslant 2048$. For this Rayleigh number there is a pitchfork bifurcation at $\hat{\beta} = 358$; the transient steady solutions at $\hat{\beta} = 256$, 512 have $N = 1.9$, 3.2 respectively, and $N \approx 3.5$ for $\hat{\beta} \geqslant 2048$. So the steady branch retains the structure sketched in figure 4(*a*).

We have also computed steady solutions as $\hat{R}$ is increased for a fixed imposed field such that $\hat{\beta} = 2048$. The pitchfork bifurcation is at $\hat{R} = 1050$ and $N$ increases monotonically with $\hat{R}$. Figure 5(*a*) shows the steady solution for $\hat{R} = 32000$ with $N = 5.67$. Compared with the solution in figure 3(*a*) the flow is more concentrated in the sinking plumes. Magnetic flux is confined to sheets surrounding the planes of symmetry and the peak field strength is 20 times the imposed flux density. The enhanced magnetic pressure causes partial evacuation of the flux sheets, where the density is locally reduced by 24%.

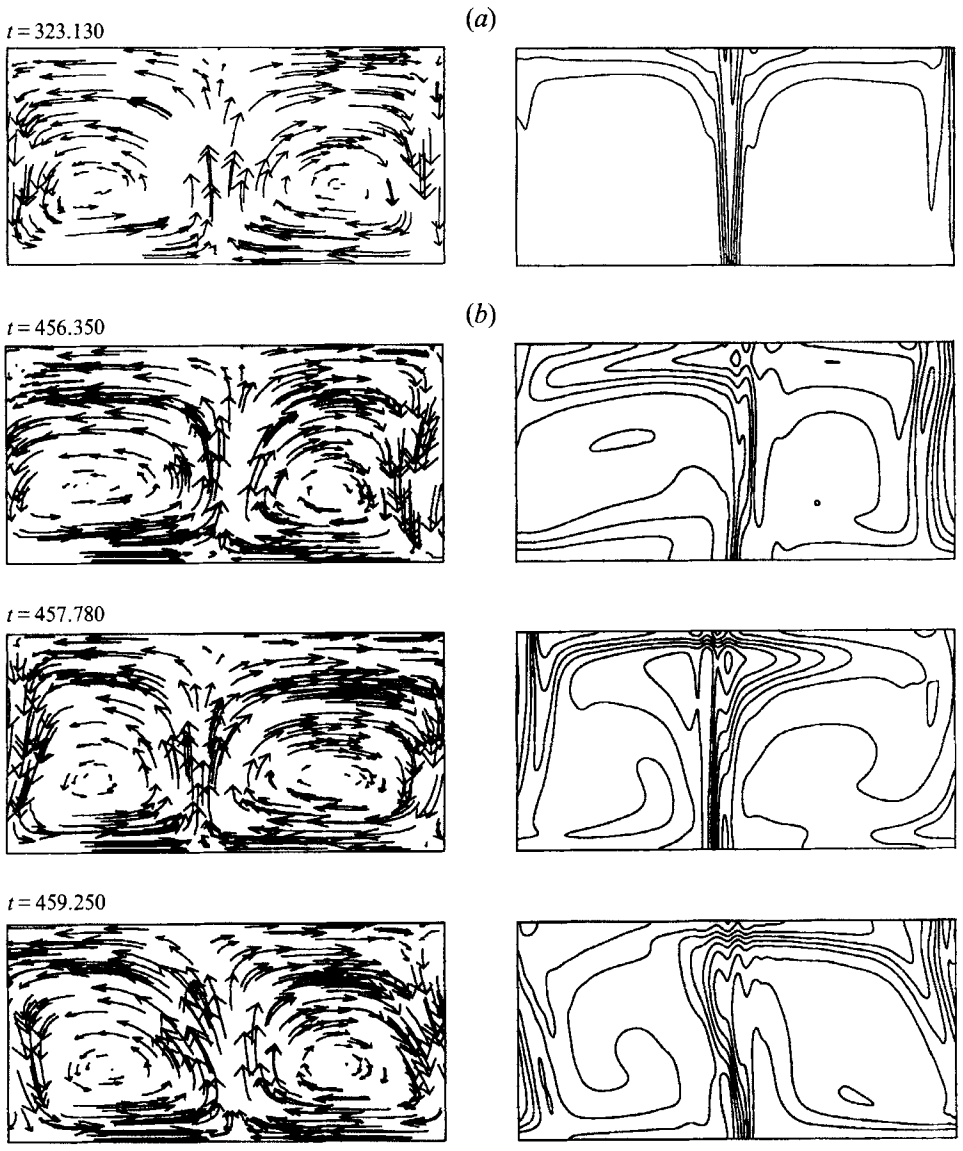


FIGURE 5. (*a*) Steady magnetoconvection at a higher Rayleigh number ($\lambda = 2$, $\beta = 2048$, $\hat{R} = 32000$). (*b*) Pulsating wave at $\hat{R} = 64000$: streamlines and fieldlines at intervals of approximately $\frac{1}{4}P$. The first and last panels are related by the broken mirror symmetry. (The spatiotemporal symmetry is clearer for $\boldsymbol{u}$ than for $\boldsymbol{B}$ since the field lines are arbitrarily chosen.)

Doubling the Rayleigh number to $\hat{R} = 64000$ yields the periodic solutions illustrated in figure 5(*b*). These oscillations are unlike anything described in Part 1, since the bifurcation breaks the mirror symmetry of figure 5(*a*) so that the solutions have the property that the flows and fields at an interval of half a temporal period are related by the broken mirror symmetry. These solutions are examples of pulsating waves, which occur generically at such a bifurcation (Landsberg & Knobloch 1991; Proctor & Weiss 1993). Unfortunately, these particular waves appear just as discretization errors are becoming significant. We have repeated the calculation after doubling the number of mesh intervals in each direction and the oscillations persist at a reduced

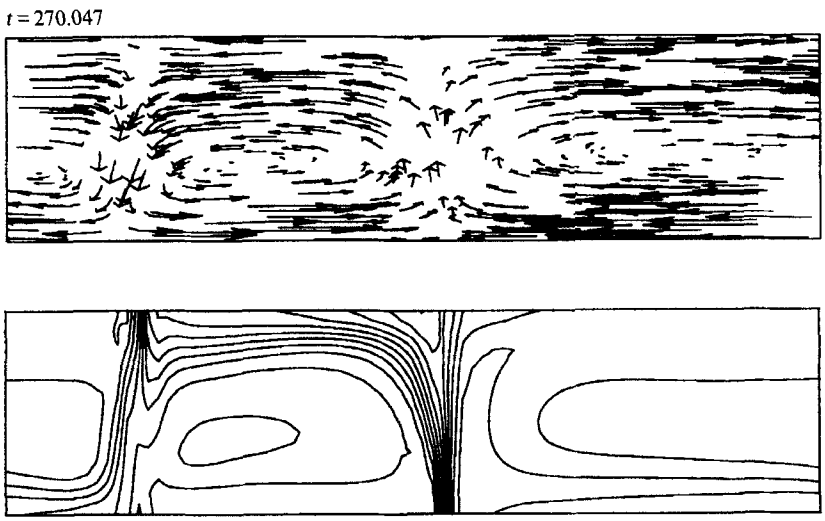


FIGURE 6. Asymmetric two-roll travelling wave for $\lambda = 4$, $\beta = 8192$, $\hat{R} = 8000$.

amplitude. At this value of $\hat{R}$ the peak value of the Mach number $M_{max} = 1.58$ and there is a possibility that shocks will form. Indeed, we know from highly accurate studies of two-dimensional compressible convection in the absence of a magnetic field that there are aperiodic oscillations of the general form shown here, accompanied by localized shocks at the top of the layer (Cattaneo, Hurlburt & Toomre 1990). Our code cannot represent such behaviour but we believe that our results are qualitatively correct and that the pulsating waves develop into the more vigorous aperiodic oscillations found by Cattaneo *et al.* (1990). This is not the only route leading to oscillations with this symmetry; an alternative is discussed in §4 below.

### 3.3. *Interactions between two-roll and four-roll solutions* ($\lambda = 4$)

Previous studies of steady compressible convection and magnetoconvection have set $\lambda = 4$ or 3 (Hurlburt *et al.* 1984; Hurlburt & Toomre 1988). We note from figure 2 that the values of $\hat{R}^{(e)}$ for $\lambda = 2$, 4 are very close for $\hat{\beta} > 2048$ and that there is a codimension-two bifurcation at $\hat{\beta} = 1953$, where $\hat{R}^{(e)} = 905$ for either aspect ratio. We have therefore investigated the effect of relaxing the lateral constraints by doubling the aspect ratio to $\lambda = 4$. Then we expect to find resonant interactions between two-roll and four-roll solutions in the weak-field regime. We describe these interactions briefly, though the interesting phenomena do not involve the magnetic field in an essential way and can also be found for non-magnetic convection.

We first set $\hat{\beta} = 8192$ and obtain solutions for different values of $\hat{R}$. The pitchfork bifurcations for $\lambda = 2$ and $\lambda = 4$ occur at $\hat{R}^{(e)} = 926$ and $\hat{R}^{(e)} = 962$. For aspect ratio $\lambda = 4$ there is a stable steady solution at $\hat{R} = 2000$ with two rolls separated by vertical planes of symmetry. At $\hat{R} = 4000$ there is a transient steady solution which gives way to asymmetric two-roll travelling waves. Similar travelling waves can also be found at $\hat{R} = 8000$ (figure 6), but with different initial conditions it is possible to obtain four mirror-symmetric rolls, identical with those computed for $\lambda = 2$ in §§3.1 and 3.2. The four-roll steady solutions are stable to long-wavelength perturbations but careful inspection shows that the travelling waves are unstable to finite-amplitude perturbations. On adding a four-roll perturbation they develop into mildly modulated waves.

Apparently, the four-roll branch bifurcates supercritically from the trivial solution

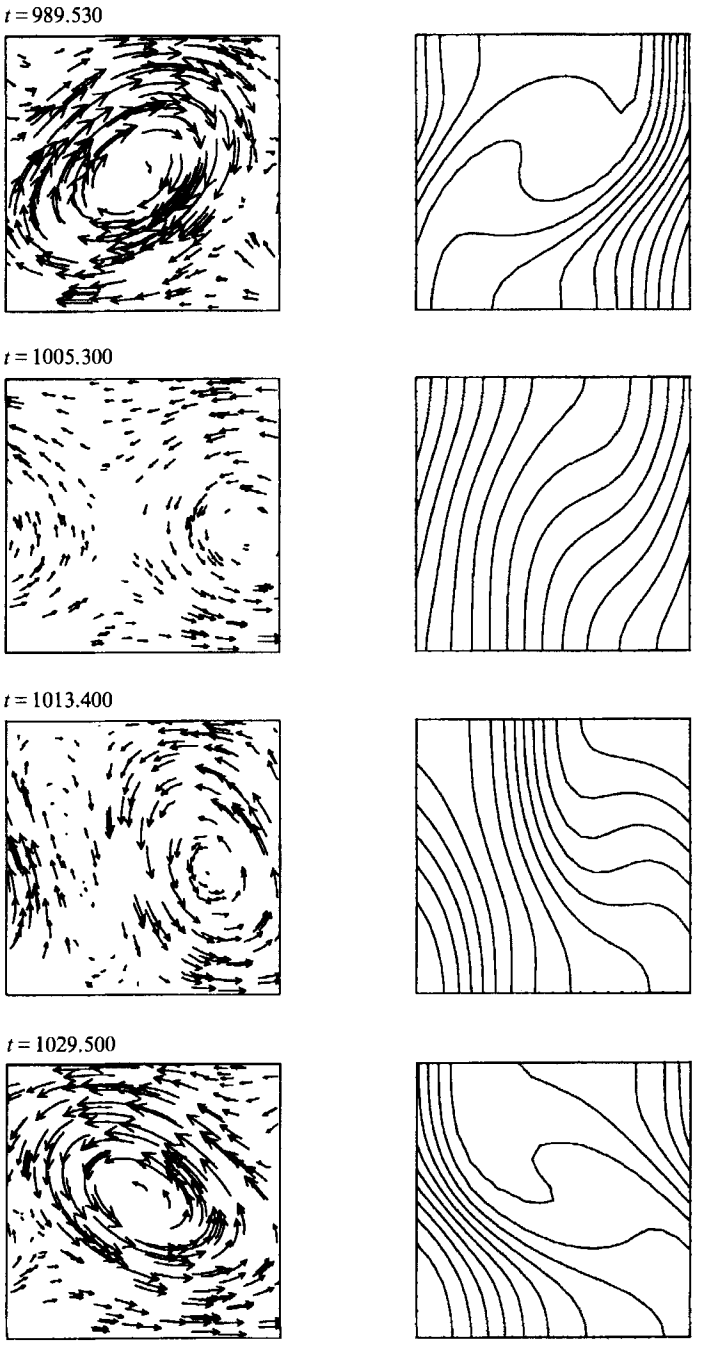


FIGURE 7. Pulsating wave for $\lambda = 1$, $\hat{R} = 8000$, $\beta = 512$. Solutions at equal intervals over half a period; the first and last are related by the spatiotemporal symmetry.

first and is followed by the two-roll branch. The latter is initially unstable to short-wavelength perturbations but soon gains stability in a pitchfork bifurcation, only to lose stability again in a second pitchfork that gives rise to travelling waves. Finally, the travelling waves undergo a subcritical Hopf bifurcation to give modulated waves.

This multistable combination – with stable four-roll steady convection, stable two-

roll travelling waves and stable modulated waves – is found at $\hat{R} = 8000$ throughout the weak-field regime, from $\hat{\beta} = 2^{20}$ ($Q = 0.11$) to $\hat{\beta} = 2048$. So it is apparently produced by purely hydrodynamic effects. Some understanding of the nature of the possible solutions near the multiple bifurcation point for the two-roll solution with horizontal wavelengths in the ratio 1:2 can be gained from the study of appropriate amplitude equations (see e.g. Dangelmayr 1986; Jones & Proctor 1987; and a very detailed study by Julien 1991). These models do not possess enough structure to account for the existence of multiple stable solutions, and further work is required before the bifurcation structure can be explained in terms of a low-order model.

When the magnetic field is dynamically important, behaviour is quite different. For $\hat{\beta} = 512$ the solution is aperiodic and displays two, three and four rolls at different phases. Results for $\hat{\beta} = 128$ and $\hat{\beta} = 32$ are likewise aperiodic, with irregular spatial structure and a characteristic timescale that decreases as the imposed field is increased. Since the corresponding solutions for $\lambda = 2$ are themselves aperiodic, this complicated behaviour is to be expected.

## 4. Streaming instabilities ($\lambda = 1$)

We now come to a form of motion that has no parallel in the investigations of Part 1, since the motion is heavily influenced by large-scale horizontal shear. These solutions are predominant when the aspect ratio of our periodic box is relatively small; the extent to which they remain relevant for wider boxes will be discussed below. It turns out that reducing the aspect ratio imposes lateral constraints that lead to richer dynamical behaviour. When $\lambda = 4$ the fundamental two-roll solution interacts with the four-roll first harmonic but when $\lambda = 1$ the mode with two pairs of stacked rolls is excited more readily than the first harmonic. Interactions between two-roll and stacked-roll solutions lead to horizontal streaming and vigorous pulsating waves. The streaming shears the magnetic field to such an extent that the Lorentz force becomes significant even in the weak-field regime. Thus there is a complicated range of phenomena to be identified and explained. In this section we describe numerical experiments: first we survey behaviour found as $\hat{\beta}$ is varied for a fixed Rayleigh number, then we focus on transitions as $\hat{R}$ (or $\hat{\beta}$) is increased for fixed $Q$. In §5 we shall develop low-order models in order to interpret these numerical results.

### 4.1. *Streaming and pulsating waves*

Once again we set $\hat{R} = 8000$. *For* $\hat{\beta} \leqslant 256$ the only stable nonlinear solutions are standing waves, as described in Part 1. There is a pitchfork bifurcation from the static solution at $\hat{\beta} = 342$ and at $\hat{\beta} = 512$ we find a transient steady solution with $N = 1.68$, which gives way to low-amplitude pulsating waves with $1.00 \leqslant N \leqslant 1.18$. The new solution is periodic and retains a spatiotemporal symmetry corresponding to reflection in vertical planes after advancing time by half a period. Figure 7 shows how the velocity and magnetic field vary during a half-cycle. This pulsating wave differs from the one displayed in figure 5, although it has the same symmetries (Proctor & Weiss 1993), in that motion is dominated by a single asymmetric eddy whose sense of rotation is reversed. The eddy is tilted and is associated with a sheared horizontal flow whose direction alternates between successive half-cycles.

Physically, we can interpret the sequence as follows. The symmetric two-roll solution is unstable to perturbations that tilt the rolls. Suppose they are tilted initially to the right. Then the rising plumes transport rightward momentum upwards, while the sinking plumes carry leftward momentum downwards. Thus the tilted rolls generate a

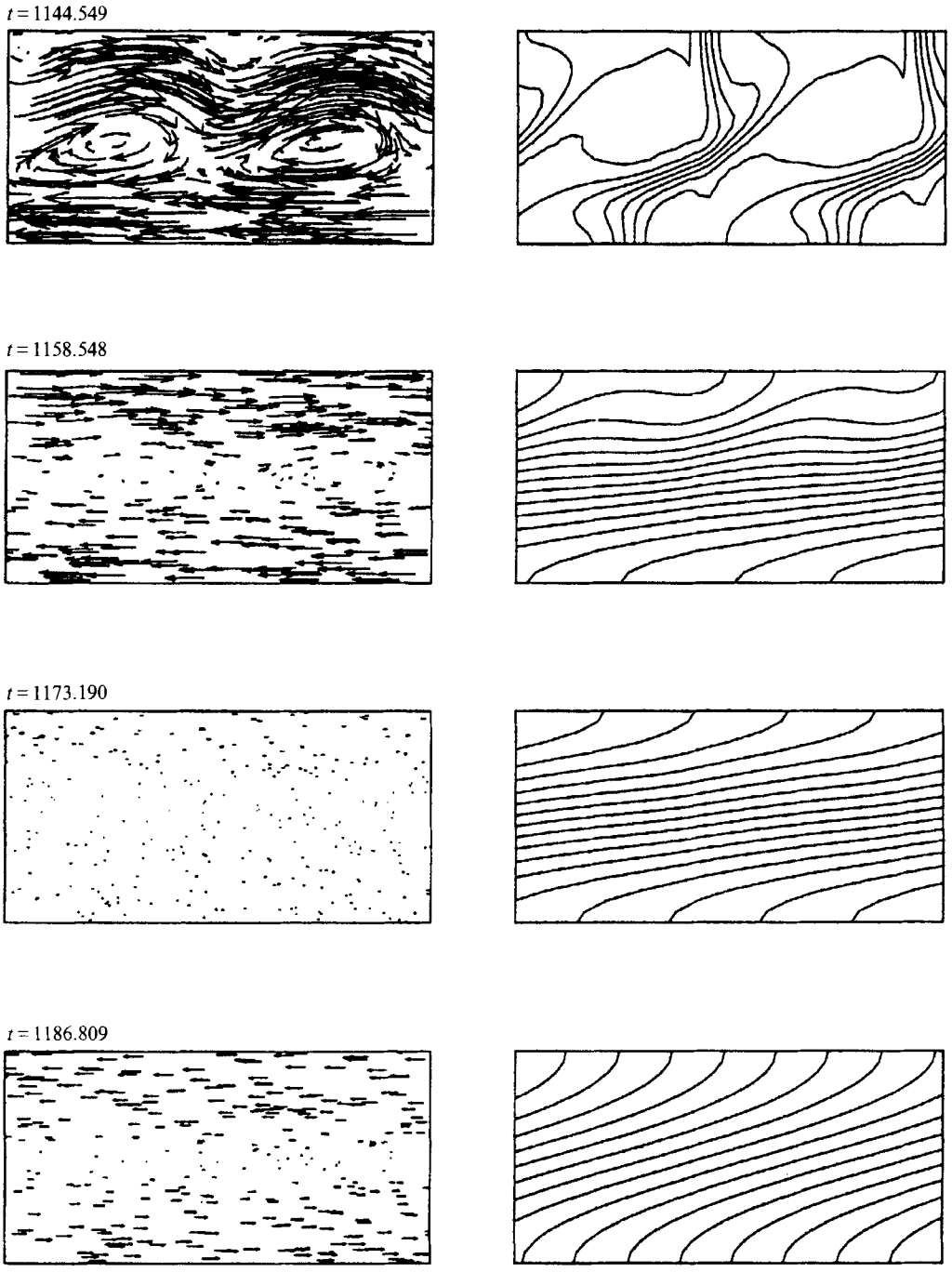


FIGURE 8. For caption see facing page.

streaming motion, with $u_x$ positive (negative) at the upper (lower) boundary. (Velocities are measured relative to the frame in which there is no net horizontal momentum.) Since $\partial u_x/\partial z < 0$ this sheared flow has negative vorticity; it therefore enhances the clockwise-rotating eddy and suppresses the anticlockwise eddy. The resulting flow distorts the magnetic field until the Lorentz force is strong enough to halt

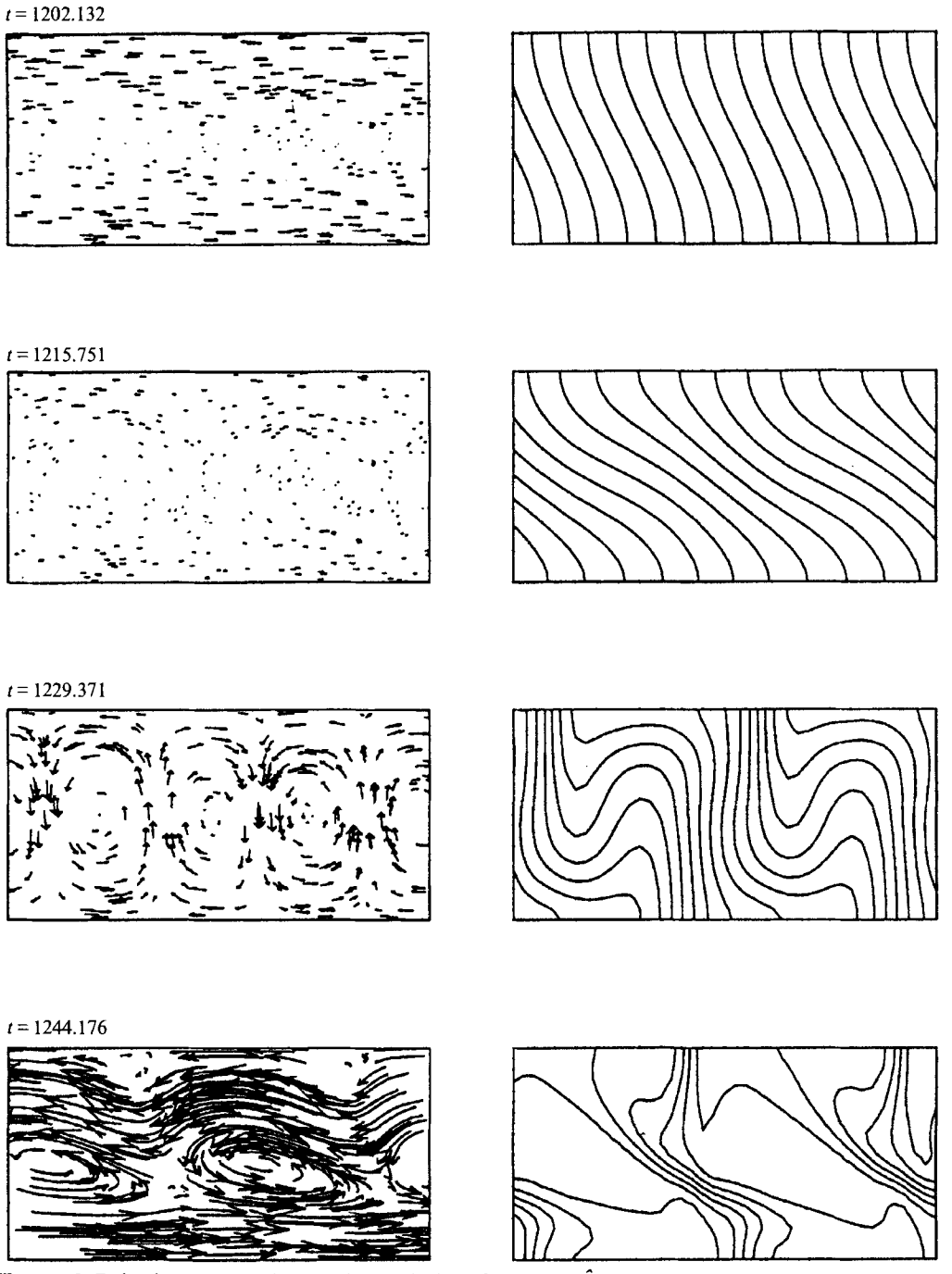


FIGURE 8. Pulsating wave and streaming: solutions for $\lambda = 1$, $\hat{R} = 8000$, $\beta = 4096$, extended over two wavelengths to clarify their structure. The panels are separated by equal intervals over a half-period. Note the long quiescent, magnetically dominated phase and the rapid burst of activity.

it, whereupon the cycle is repeated in reverse. This description shows that we are dealing with a new type of hydromagnetic oscillation (Matthews *et al.* 1993).

Behaviour at higher Rayleigh numbers is complicated by interactions between pulsating waves and standing waves. They appear most clearly in the strong-field

regime discussed in Part 1. For $\hat{\beta} = 64$ there are stable standing waves at $\hat{R} = 8000$ and $\hat{R} = 16000$. Between this value and $\hat{R} = 32000$ these solutions must lose their mirror symmetry in a Hopf bifurcation, since quasi-periodic modulated waves are found at the higher value (see figure 8*a* of Part 1). The latter are of mixed-mode type, combining features of standing waves and pulsating waves but lacking the symmetries of either. Doubling the Rayleigh number to $\hat{R} = 64000$ yields the aperiodic modulated waves illustrated in figures 8(*b*) and 8(*c*) of Part 1. As the imposed field is decreased these interactions occur at lower Rayleigh numbers: for $\hat{\beta} = 128$ the standing waves at $\hat{R} = 8000$ develop into asymmetric quasi-periodic oscillations at $\hat{R} = 16000$ and aperiodic motion at $\hat{R} = 32000$; for $\hat{\beta} = 512$ aperiodic modulated waves are already present at $\hat{R} = 16000$.

At $\hat{R} = 8000$ there are pulsating waves for $512 \leqslant \hat{\beta} \leqslant 2^{16}$ ($222 \geqslant Q \geqslant 1.74$). The form of these solutions changes as the imposed magnetic field is decreased. For $\hat{\beta} = 1024$ the pulsating wave solution is similar to that described above but it becomes unstable to perturbations that break its spatiotemporal symmetry, giving rise to a modulated wave which is periodic in a uniformly moving frame. (Increasing the Rayleigh number to $\hat{R} = 10000$ yields an aperiodically modulated wave – see §4.2 below.) At $\hat{\beta} = 2048$ the modulated wave seems to have undergone a period-doubling bifurcation by $\hat{R} = 8000$. Stable pulsating waves appear once more at $\hat{\beta} = 4096$ but now they are more spasmodic and have a more dramatic form, as shown in figure 8. The single eddy develops into vigorous streaming motion, which kills the convective rolls and rapidly sweeps the field aside until it is almost horizontal. Although the imposed field is weak ($Q = 28$) the distorted field eventually becomes strong enough to reverse the streaming motion. Next comes a quasi-static phase, with a weak reversed flow, during which the field lines slowly regain an approximately vertical orientation, while the temperature is horizontally stratified. Then there is a burst of activity, which is illustrated in more detail in figure 9: convection rolls develop rapidly and tilt to give a single reversed eddy, after which the cycle proceeds as before but with an oppositely directed shear. Once again the oscillations rely on the curvature force exerted by the magnetic field. As the imposed field is progressively reduced, to $\hat{\beta} = 2^{16}$, the same pattern persists. The oscillations grow more intermittent, with longer intervals between the bursts of activity, and the field has to be amplified by a larger factor before the motion is reversed.

### 4.2. *Pulsating waves and modulated waves*

In order to understand the development of pulsating waves we need to start from the static solution and to follow the bifurcation sequence as the Rayleigh number is increased. For the initial bifurcation at $\hat{R}^{(e)}$ we choose a field of intermediate strength; in order to keep clear of the line of pitchfork bifurcations – which follow a line of constant $\hat{\beta}$ in figure 2 – it is preferable to fix $Q$ rather than $\hat{\beta}$. We choose the line that passes through the point with $\hat{R} = 8000$, $\hat{\beta} = 1024$ and therefore set $Q = 111.1$. Then the initial bifurcation at $\hat{R}^{(e)} = 4795$ is at a safe distance from the Takens–Bogdanov bifurcation at $Q = 230$, $\hat{R} = 6900$.

At $\hat{R} = 4900$ we obtain a low-amplitude steady solution, which remains stable up to $\hat{R} = 5100$ ($N = 1.0154$). For $\hat{R} = 5100$ it is also possible to find a stable travelling wave solution ($N = 1.0465$) which can be followed down to $\hat{R} = 5000$. It is important to note that these waves arise in a quite distinct manner from the travelling waves in the strong-field case; the latter appear at a primary Hopf bifurcation from the static state while the former arise through a pitchfork bifurcation from a steady solution, as discussed below. For $\hat{R} = 5200$ the only attracting solution is a modulated wave ($1.041 \leqslant N \leqslant 1.056$) which fluctuates about the unstable travelling wave without reversing the

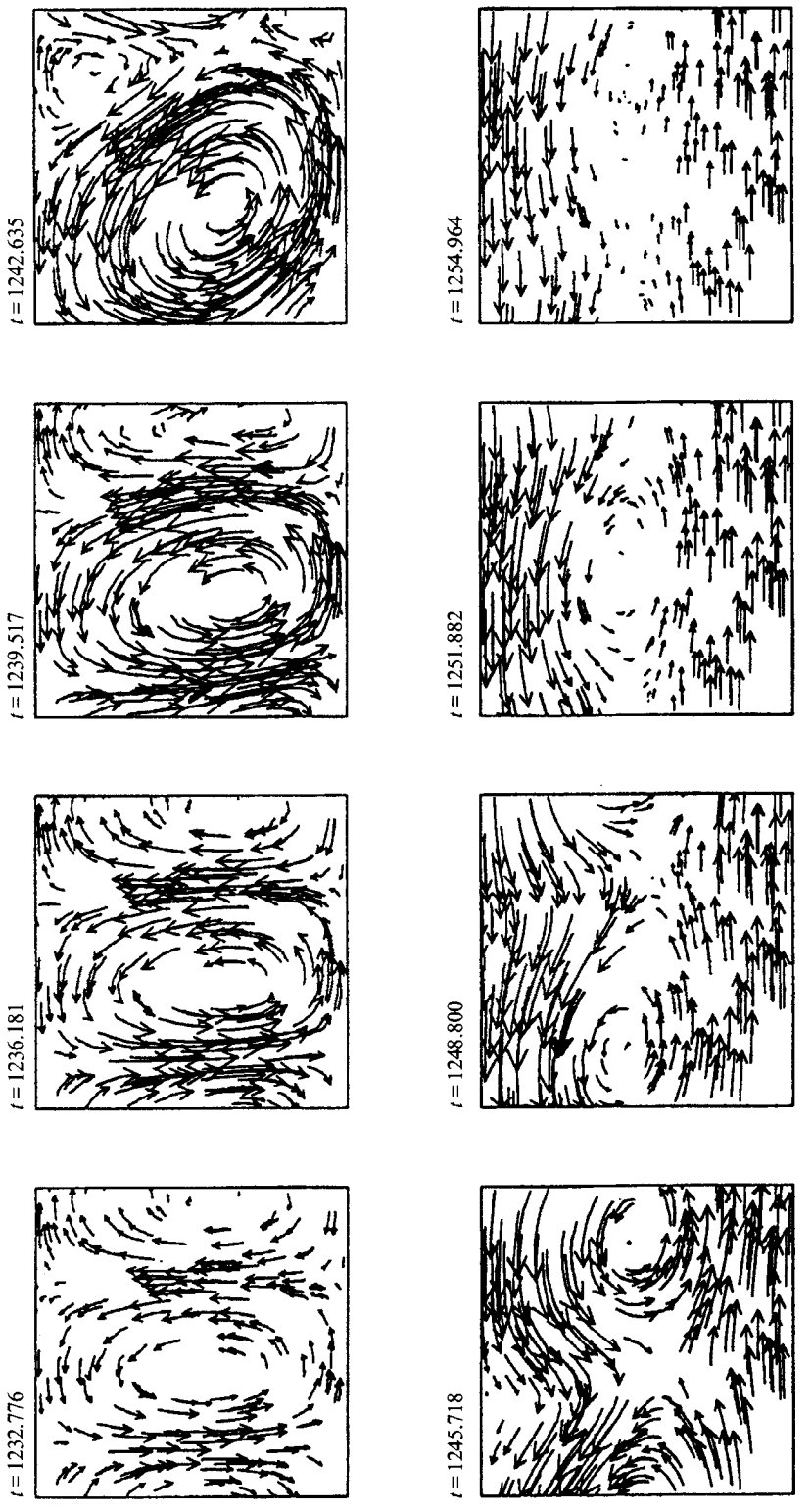


FIGURE 9. As for figure 8, but showing the development of the velocity field during the brief active phase. The frames are separated by an interval $\Delta t \approx 0.016P$, starting $\Delta t$ later than the last panel of figure 8. Note the almost symmetrical convection rolls, which tilt, generate shear, become strongly asymmetric and then decay, leaving a vigorous streaming motion.

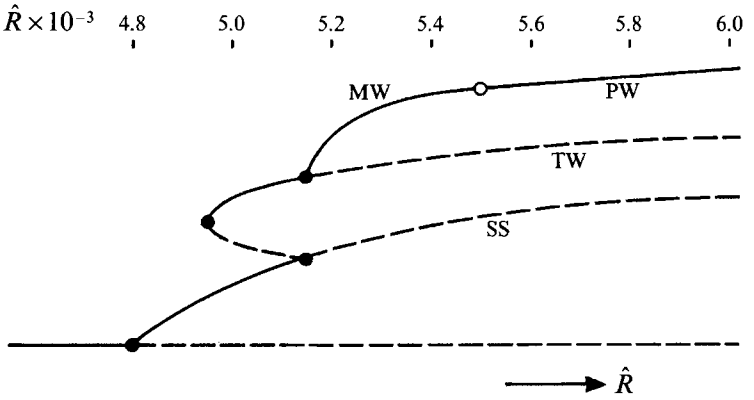


FIGURE 10. Bifurcation diagram for $\lambda = 1$, $Q = 111.1$. The trivial solution loses stability in a pitchfork bifurcation, giving a stable SS; a subcritical secondary pitchfork gives rise to TW, which gain stability in a saddle-node bifurcation but lose it again in a Hopf bifurcation, leading to MW; stability is transferred to pulsating waves (PW) at a homoclinic gluing bifurcation.

velocity. Stable modulated waves persist to $\hat{R} = 5400$. At $\hat{R} = 5500$ there is a chaotic modulated wave, with irregular reversals of the flow and a mean period $\bar{P} = 152$. At $\hat{R} = 5600$ there is again a modulated wave, with periodic reversals and $\bar{P} = 138$. For $\hat{R} = 6000$ we find a stable pulsating wave with spatiotemporal symmetry and a period $\bar{P} = 112$; this can be followed up to $\hat{R} = 7000$ ($1.00 \leqslant N \leqslant 1.15$, $\bar{P} = 91$). At $\hat{R} = 8000$ the pulsating wave gradually loses its symmetry and develops into a modulated wave, as mentioned in §4.1 above. The modulated wave is periodic in a moving frame but – unlike the wave at $\hat{R} = 5400$ – there are reversals of the flow. Finally, at $\hat{R} = 10000$ there is a transient pulsating wave which eventually becomes chaotic.

This sequence of numerical experiments allows us to construct the bifurcation diagram in figure 10. The initial stationary bifurcation is followed by a branch of steady solutions with mirror-symmetric rolls. These solutions are initially stable but their symmetry is broken in a subcritical pitchfork bifurcation at $\hat{R} \approx 5150$, which gives rise to travelling waves. The branch of travelling waves gains stability in a saddle-node bifurcation at $\hat{R} \approx 4950$ but loses it again in a Hopf bifurcation at $\hat{R} \approx 5150$, shedding a branch of modulated waves. The modulated waves continue to $\hat{R} \approx 5500$, where there is a homoclinic gluing bifurcation. This global bifurcation is associated with complicated chaotic behaviour (Matthews *et al.* 1994*a*). From it emerges a branch of pulsating waves with eddies that reverse direction after each half-period, and a period $\bar{P}$ that decreases rapidly with increasing $\hat{R}$. These waves can be followed up to $\hat{R} = 10000$ but around $\hat{R} = 8000$ they undergo a symmetry-breaking bifurcation that gives rise to a different type of modulated wave. Subsequently there must be other bifurcations leading to more exotic oscillatory behaviour but those developments need not concern us here.

Figure 10 shows a sequence of bifurcations, starting from the static solution and ending with pulsating waves. This whole sequence can be interpreted by relating it to the low-order model systems that we shall discuss in §5.

### 4.3. *Symmetry-breaking in the kinematic regime* ($Q \ll 1$)

Previous studies of nonlinear compressible convection in the absence of a magnetic field have reported a variety of time-dependent behaviour for aspect ratios that are small (Hurlburt *et al.* 1984; Ginet & Sudan 1987; Lantz 1994). Hurlburt *et al.* illustrate an aperiodic solution, with vigorous streaming but no reversals of the flow, for a

strongly stratified layer with $\lambda = 0.5$. Ginet & Sudan made a systematic study of convection, again in a strongly stratified layer ($z_0 = 0.14$, $m = 1.49$) with $\lambda = 1$. They found steady, periodic, quasi-periodic and chaotic behaviour, with streaming and a single asymmetric eddy but no reversal of the flow. They adopted the anelastic approximation and varied the Rayleigh number by keeping $\bar{K}$ constant and reducing $\sigma$; although we cannot make a direct comparison between our results and theirs, it is of interest to discover how far their solutions relate to the behaviour that we have described above.

We have therefore investigated convection with $\lambda = 1$ and $Q = 0.1085$ (a value chosen so that $\hat{\beta} = 2^{20}$ at $\hat{R} = 8000$). Then the initial bifurcation at $\hat{R}^{(e)} = 3204$ gives rise to mirror-symmetric rolls. With our code we find a feebly convecting solution at $\hat{R} = 3160$ with $N = 1.014$. Close inspection shows that the streaklines are very slightly asymmetric. At $\hat{R} = 3200$ there are slowly drifting, slightly asymmetric travelling waves ($N = 1.016$) and by $\hat{R} = 3300$ the asymmetry and drift are more pronounced. We infer that there is again a subcritical pitchfork bifurcation from the branch of steady solutions giving rise to a branch of travelling waves with a turning point at $\hat{R} \approx 3100 < \hat{R}^{(e)}$. Around $\hat{R} = 3350$ there is a Hopf bifurcation, yielding modulated waves. As $\hat{R}$ is further increased, these waves become intermittent, with short bursts of activity separated by long quiescent intervals. Once again, convective rolls develop into a single asymmetric eddy, which generates a sheared flow that gradually decays; but now the magnetic field is too weak to reverse the streaming motion. The modulated waves persist to $\hat{R} = 6000$ ($1.00 \leqslant N \leqslant 1.18$). Apparently there is a second Hopf bifurcation around $\hat{R} = 7000$ at which the travelling waves regain stability. At $\hat{R} = 8000$ the modulation gradually decays to give a travelling wave with $N = 1.026$. Thus there is a marked contrast between the travelling wave for $\lambda = 1$ and the steady solution for $\lambda = 2$, which has a reasonable amplitude ($N = 3.6$) at $\hat{R} = 8000$. For $\hat{R} = 10000$ we again find a travelling wave with slowly decaying modulation but at $\hat{R} = 12000$ there is a modulated wave with long-period oscillations in the Nusselt number. At $\hat{R} = 16000$ this slow modulation dies away and is replaced by rapid modulation of the drifting wave.

From these results we surmise that the transition from steady to periodic behaviour reported by Ginet & Sudan (1987) is in fact a transition from travelling waves to modulated waves, and that it is preceded by a transition from steady convection to travelling waves, with a consequent loss of symmetry (cf. Lantz 1994). Indeed, symmetry considerations preclude a direct transition from steady mirror-symmetric rolls to modulated waves (Proctor & Weiss 1993). The subsequent transitions from modulated waves to quasi-periodic modulation and to chaotic motion involve two very disparate timescales. We are unable at present to clarify the processes involved, since these transitions occur at Rayleigh numbers in the range $14 < \hat{R}/\hat{R}^{(e)} < 80$, which are higher than any that we have so far investigated.

It is noteworthy that the pulsating waves, with their reversals of the shear, seem only to be accessible from the travelling waves when the field is sufficiently strong. The key to the difference is the nature of the decay of the shear, and is discussed below in the context of a low-order model system.

## 5. Simple low-order models for the streaming instabilities

The sequences of bifurcations described above may be partially understood by the construction and investigation of low-order systems of ordinary differential equations whose dependent variables represent the important features of the flows and fields.

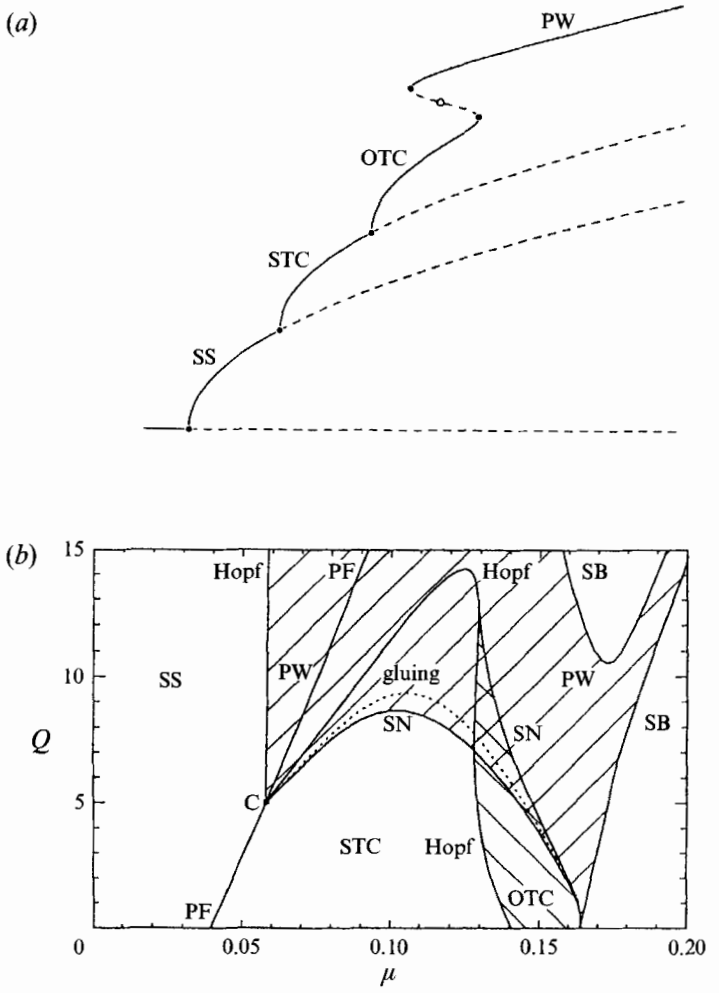


FIGURE 11. Low-order models of streaming instabilities in Boussinesq magnetoconvection (cf. Rucklidge & Matthews 1993, 1994). (*a*) Bifurcation diagram, showing the transition from steady symmetric convection to steady tilted convection (STC) to oscillatory tilted convection (OTC) and, via a global bifurcation, to PW. Note the similarity to figure 10. (*b*) Bifurcation structure in the $(\mu, Q)$-plane, showing solutions that are stable in different regions; stable PW are found throughout the shaded region. (After Matthews *et al.* 1993.)

Such models are often best obtained by means of a severe truncation of the governing equations in some Fourier or Galerkin representation. When the underlying stability problem cannot be solved analytically, the utility of such a scheme is reduced and direct selection of the appropriate nonlinear terms, having regard to appropriate symmetry considerations, becomes preferable. The method has been used with success, however, to explain transitions in double convection with stress-free boundaries and no-flux lateral boundary conditions (Knobloch, Weiss & Da Costa 1981; Knobloch & Proctor 1981; Knobloch, Proctor & Weiss 1992). Howard & Krishnamurti (1986) were the first to give an analytical description of the instabilities of non-magnetic two-dimensional Boussinesq convection coupled with horizontal streaming flows. They recognized that the crucial ingredients in the instability were the interaction between two different convective modes with the same horizontal wavenumber but different vertical structure;

no shear is generated when these modes are in phase (i.e. have the same nodes in the horizontal) but when there is a phase difference the interaction drives a shearing flow, which then interacts with and couples together the two convective modes. The Howard–Krishnamurti model is sixth order: the mean horizontal flow and mean temperature profile are each represented by a single mode, while the two convective cellular flows have two modes each. Hughes & Proctor (1990) recognized that the basic dynamics could be explained by just three equations, and showed how to perform the reduction when the aspect ratio is small. (This reduced description does not include perturbations to the mean temperature, which would not significantly affect their solutions.) These studies show clearly that a streaming instability can arise in the non-magnetic case but the oscillatory reversals of the shear, which figure so prominently in the numerical experiments, do not occur commonly here. In the presence of a magnetic field, streaming is affected by the Lorentz force and takes the form of decaying Alfvén waves rather than viscously decaying shear (Matthews *et al.* 1993). We can therefore extend the Howard–Krishnamurti model by incorporating the effects of a vertical imposed field. The resulting eleventh-order system has been derived for the Boussinesq problem by Rucklidge & Matthews (1993, 1994); these papers are henceforth referred to collectively as RM and we shall rely on several of their results in what follows. By taking the limit of thin cells, RM obtain a fifth-order real system. For later convenience we express it here in complex form.

The starting point for our model is a complexification of that in RM. To begin with, we assume that the Boussinesq approximation holds (see e.g. Proctor & Weiss 1982). The governing equations are then considerably simpler than those for a compressible atmosphere, and the eigenfunctions can be expressed in terms of trigonometric functions. Because of the assumed constancy of fluid properties in the Boussinesq equations, there is a symmetry about the midpoint of the layer (Proctor & Weiss 1993), so that the eigenfunctions are either even or odd about the midpoint. The extended model then consists of an 'even' convective mode with e.g. temperature perturbation $Ae^{ikx}\sin\pi z$, an 'odd' mode $Ce^{ikx}\sin 2\pi z$, a horizontal shear flow $B\cos\pi z$, a mean horizontal magnetic field $G\cos\pi z$ and a mean temperature perturbation $E\sin 2\pi z$. Here $A$ and $C$ are complex in general while $B$, $G$ and $E$ are real. Substituting these equations into the governing Boussinesq equations, and making the appropriate rescalings, we obtain

$$\dot{A} = \mu A + AE + \mathrm{i}BC, \tag{5.1}$$

$$\dot{B} = \frac{1}{4}\left[\frac{3(1+\sigma)}{\sigma}\,\mathrm{Im}\,(\bar{A}C) - \sigma\left(B + \frac{Q}{\pi^2}G\right)\right], \tag{5.2}$$

$$\dot{C} = \left[\mu - \frac{9\sigma}{4(1+\sigma)}\right]C + \mathrm{i}AB, \tag{5.3}$$

$$\dot{E} = -E - |A|^2, \tag{5.4}$$

$$\dot{G} = \tfrac{1}{4}\zeta(B-G), \tag{5.5}$$

where $\mu$ is a measure of the supercritical Rayleigh number. An important feature of this system is that, because of the symmetries of the modes, the quadratic terms in $B$ do not induce self-coupling between the convective modes (so that e.g. there is no $AB$-term in the $A$-equation). In consequence the equations have an invariant subspace in which $\arg(C) = \arg(A) + \frac{1}{2}\pi$. It can be shown that $(\mathrm{d}/\mathrm{d}t)[\arg(A)] = 0$ in this subspace, so that (5.1)–(5.5) can be reduced to five *real* equations. RM note that in an appropriate

coordinate system we can describe solutions in this subspace as possessing point symmetry (Proctor & Weiss 1993). This symmetry prevents the initial instability to shear from resulting in travelling waves. The subspace can become unstable, however, at sufficiently large $\mu$ (Julien *et al.* 1993); then travelling disturbances become the norm. A proper description of these disturbances should include other modes. However, we do not expect these modes to be important in a stratified layer, where there is no point symmetry to be broken.

Before showing how the above system must be modified to incorporate non-Boussinesq effects, we summarize some of RM's more suggestive results. They integrated the system (5.1)–(5.5) in the real subspace for $Q = 4$, $\sigma = 0.5$, $\zeta = 0.2$ and found the following bifurcation sequence, illustrated in figure 11(*a*). The initial bifurcation at $\mu = 0$ is to a state with $B = C = G = 0$, corresponding to steady-state convection with mirror-symmetric rolls (SS). As $\mu$ is increased this state suffers a pitchfork bifurcation to a new steady state in which all variables are now non-zero. This corresponds to convection with steady tilted cells (STC); every other cell is now larger than its neighbour but because of the point symmetry there is no travelling. A further Hopf bifurcation leads to the tilt becoming vacillatory (OTC); after a gluing bifurcation of very complex type the shear and tilt actually change sign, leading to pulsating waves (PW) (see also Matthews *et al.* 1993). The corresponding 'unfolding diagram' in $(\mu, Q)$-space is given in figure 11(*b*), showing that PW solutions may also arise directly at a Hopf bifurcation from the SS branch. It is to be noted that the PW can arise by this mechanism only when the field strength represented by $Q$ is sufficiently strong. This is connected with the decay modes of the horizontal shear, which are real in the kinematic limit but can be complex for larger $Q$, allowing the sign of the shear to change during the motion. This corroborates the observed difference between the non-magnetic and magnetic results described above.

How are these results to be related to the compressible results described earlier? It turns out that we can model the effects of compressibility very simply, by noting that the difference of *parity* between the convective modes in the $A$ and $C$ equations is now broken. In consequence there is nothing on the grounds of symmetry to rule out self-coupling terms in (5.1) and (5.3), which will now take the form

$$\dot{A} = \ldots\ldots + \mathrm{i}\delta_A BA, \tag{5.6}$$

$$\dot{C} = \ldots\ldots + \mathrm{i}\delta_C BC, \tag{5.7}$$

where the dots denote the existing terms in (5.1)–(5.3). For weak compressibility the other coefficients in the equations will be almost unchanged, so we can leave them as they are, while $\delta_A, \delta_C$ will be small. (While the stratification will in general induce other small coupling terms, these will not introduce any effects that are not already present in the simple model above.) The effect of these terms is to eliminate point symmetry when $B$ is non-zero, so any tilt of the convection cells is accompanied by secular change of the phases of $A$ and $C$, leading to drift of the pattern; although the bifurcation from the SS solution is still of pitchfork type, the bifurcated pattern has the same symmetries as the travelling waves (TW) that can arise, through a primary Hopf bifurcation, in other parameter ranges (see Part 1). It is easy to see that we can find bifurcated solutions with $A$, $C \propto \mathrm{e}^{\mathrm{i}\omega t}$ and $B$, $E$, $G$ independent of time.

In general the dependence of $\omega$ on the parameters is very messy, but in the special case $\delta_A = \delta_C$ we can make the substitutions $A = \tilde{A}\,\mathrm{e}^{\mathrm{i}\delta_A Bt}$, $C = \tilde{C}\,\mathrm{e}^{\mathrm{i}\delta_A Bt}$ and then (5.1)–(5.5) are recovered with $\tilde{A}, \tilde{C}$ replacing $A, C$. Thus the phase speed of the pattern is $B\delta_A$ and the bifurcation structure is identical with that shown in figure 11, except that

the solution branches now have a different interpretation. Because of the lack of up–down symmetry the pattern drifts with phase velocity $\delta_A B/k$ when the streaming flow is present. Thus the STC solutions, which were steady in the Boussinesq case, now travel at constant speed; moreover, they have the same symmetries as the travelling wave (TW) solutions that arise by a quite different mechanism, involving a Hopf bifurcation from the trivial solution, in both the compressible and Boussinesq problems when $\zeta < 1$ and $Q$ is sufficiently large. By the same token the OTC solutions now become quasi-periodic modulated waves (MW), with a periodic phase velocity. After the transition that gives pulsating waves in the Boussinesq case, the left–right symmetry is restored; so there is no preferred direction even when $\delta_A \neq 0$, and the realized solutions exhibit alternating shear, with the convection cells being advected alternately in opposite directions as $B$ changes sign.

When $\delta_A \neq \delta_C$ we cannot precisely identify the bifurcations in the two cases, but it is clear that the transitions from steady-state convection through travelling waves to modulated waves, being standard codimension-one bifurcations, will not be affected. The very complex transition to PW solutions described by RM, which depends on the point symmetry that is generically destroyed in the compressible case, may require a different interpretation in this case, but the general notion of a gluing bifurcation clearly remains valid. We may therefore regard the observed transitions as being adequately modelled, and indeed the sequence of bifurcations deduced from the numerical experiments in figure 10 is identical with that in figure 11 (*a*) except that the bifurcation to TW is subcritical in the former case. There is a strong case for further investigation of the model when $\delta_A \neq \delta_C$ to discover other, less accessible, transitions that may be hiding in the full compressible dynamics, though such a discussion lies outside the scope of this paper, which is concerned with the interpretation of numerical experiments. It is nonetheless gratifying that the simple adjustment to RM's existing model that we exhibit here can reproduce the changes in the symmetries of the solution at bifurcation points. The utility of having such a model to hand is that it can be exhaustively investigated. Previous comparisons of low-order models with the solutions of the full p.d.e.'s have always yielded mutually useful information, and the present case is no exception.

There is evidence from some of the runs reported on above that the period of the pulsations can be very long in the weak-field regime, with long intervals when the flow is almost horizontal. This is presumably associated with a discrepancy between the (rapid) time for growth of cellular convection ($O(\mu^{-1})$ in our model) and that of the response of the horizontal flow, which increases as $Q$ decreases. The observed intermittency is due to the latter time being long compared with $\mu^{-1}$: as $Q$ increases the enhanced restoring force reduces the discrepancy. All this is consistent with the numerical experiments, but it should be noted that the intermittency here differs from that of Hughes & Proctor (1990) who concentrated on the case where $\mu^{-1}$ is much larger than other timescales.

## 6. Discussion

In this paper we have conducted a thorough survey of the secondary instabilities that lead to time-dependent magnetoconvection. While the results for wider boxes yield few surprises, the small aspect ratio calculations have allowed us to investigate the phenomenon of pulsating waves, which are dramatically different from the usual periodic solutions to be found near onset. We have clarified the mechanisms by which these waves arise, and related them to the underlying symmetries of the problem. In

this way, they can be seen as exemplars of a type of motion that can occur in many physical systems under the correct conditions. Although the bifurcation sequence that ultimately results in pulsating waves is extremely complex, it can be understood by reference to a truncated low-order system that has been extensively investigated elsewhere. This allows the gaps in the bifurcation sequence to be filled, especially in the difficult region where the modulated waves give way to pulsating waves. We have shown how even a weak imposed field can make possible the crucial transition to oscillatory shear that is the hallmark of the pulsating wave; this rather surprising effect justifies our consideration of the weak-field regime. Our runs have all made use of the 'illustrative' magnetic boundary condition $B_x = 0$ on the horizontal boundaries. These conditions have been almost universally employed in astrophysically motivated studies of magnetoconvection, as they make as few assumptions as possible about conditions outside the layer. One might alternatively have used 'frozen-field' conditions (no boundary footpoint motion) or matched the field to an external potential field. In the former case, the effect of the curvature forces on the pulsations would be much stronger, and so there would certainly be quantitative differences in the parameter values bounding the various regimes, though the symmetries of the problem would not change and so we can see no new phenomena appearing. The potential field is in some sense intermediate between the perfectly conducting and vertical field cases. All things considered, we believe that our model is typical of behaviour in a variety of cases.

In the parameter ranges selected, we have only been able to find coherent streaming instabilities for rather narrow computational boxes. It is known, however, that for strong fields convection prefers these small aspect ratios (see e.g. Proctor 1986), and the importance of the streaming flows is probably not associated with the fact that the box is *constrained* to be narrow, but with the narrowness itself. The study of the onset of convection for large values of $Q$ in wide boxes has not, curiously, been attempted to date, but it is intended to attack the problem soon in the full three-dimensional case. In any event, the interest of the problem extends beyond magnetoconvection, since modulated waves and pulsating waves that are associated with streaming arise in so many other contexts.

Of course, all these transitions occur in a constrained two-dimensional geometry. Far more complex phenomena are to be expected in a fully three-dimensional computation. Numerical experiments on three-dimensional compressible magneto-convection are at present being carried out (Matthews 1993; Matthews *et al.* 1994*b*). In the weak-field regime two-dimensional rolls are indeed stable near the initial bifurcation. These computations have already revealed a fascinating new range of solutions. In particular, streaming instabilities develop into 'alternating pulsating waves', in which the direction of streaming alternates between two orthogonal directions (Matthews *et al.* 1994*a*). The bifurcations that lead to these solutions have not yet been identified, but are clearly complicated. It is thus encouraging that, although our two-dimensional solutions are highly over-simplified, they do give an idea of the types of flows to be expected in three-dimensional calculations.

We gratefully acknowledge helpful conversations with Gregory Ginet, Edgar Knobloch, Paul Matthews and Alastair Rucklidge, as well as constructive comments from the referees. This work was supported by the UK SERC.

## Appendix. Summary of numerical results

In this appendix we list the different series of runs that have been carried out, with a brief qualitative description of the solutions found. Further details are given in the text.

$\lambda = 1$

$\hat{R} = 8000$

$\hat{\beta} = 32, 64, 128, 256$ (SW); $\hat{\beta} = 512$ (PW); $\hat{\beta} = 1024, 2048$ (MW);

$\hat{\beta} = 4096, 8192, 2^{16}$ (PW); $\hat{\beta} = 2^{20}$ (TW).

$Q = 111.125$

$\hat{R} = 4900, 5000, 5100$ (SS); $\hat{R} = 5000, 5100$ (TW); $\hat{R} = 5200, 5300, 5400, 5600$ (MW);

$\hat{R} = 5500$ (aperiodic); $\hat{R} = 6000, 7000$ (PW); $\hat{R} = 8000$ (transient PW, MW);

$\hat{R} = 10000$ (transient PW, aperiodic).

$\hat{\beta} = 2^{20}$ (kinematic)

$\hat{R} = 3160, 3200, 3300$ (TW); $\hat{R} = 3350, 3400, 3500, 4000, 6000$ (MW);

$\hat{R} = 8000, 10000$ (TW); $\hat{R} = 12000, 16000$ (MW).

$\lambda = 2$

$\hat{R} = 1750$

$Q = 30$ (transient SS, TW); $Q = 1$ (SS *or* TW).

$\hat{R} = 2000$

$\hat{\beta} = 128, 256$ (SW); $\hat{\beta} = 512, 1024$ (transient SS, TW);

$\hat{\beta} = 2048, 4096, 8192, 2^{14}, 2^{15}, 2^{20}$ (SS).

$\hat{R} = 4000$

$\hat{\beta} = 128$ (SW); $\hat{\beta} = 256$ (transient SS, aperiodic).

$\hat{R} = 8000$

$\hat{\beta} = 32, 128$ (aperiodic); $\hat{\beta} = 256, 512, 1024$ (transient SS, aperiodic);

$\hat{\beta} = 2048, 8192, 2^{15}, 2^{20}$ (SS).

$\hat{\beta} = 2048$

$\hat{R} = 2000, 4000, 8000, 16000, 32000$ (SS); $\hat{R} = 64000$ (PW).

$\lambda = 4$

$\hat{\beta} = 8192$

$\hat{R} = 2000$ (SS); $\hat{R} = 4000$ (TW); $\hat{R} = 8000$ (TW, MW *and* 4-roll SS).

$\hat{R} = 8000$

$\hat{\beta} = 32, 128, 512$ (aperiodic); $\hat{\beta} = 2048, 8192, 2^{15}, 2^{20}$ (TW, MW *and* 4-roll SS).

## REFERENCES


CATTANEO, F. 1984 Compressible magnetoconvection. PhD dissertation, University of Cambridge.

CATTANEO, F., HURLBURT, N. E. & TOOMRE, J. 1990 Supersonic convection. *Astrophys. J.* **349**, L63–L66.

COUGHLIN, K. T. & MARCUS, P. S. 1992*a* Modulated waves in Taylor–Couette flow. Part 1. Analysis. *J. Fluid Mech.* **234**, 1–18.

COUGHLIN, K. T. & MARCUS, P. S. 1992*b* Modulated waves in Taylor–Couette flow. Part 2. Numerical simulation. *J. Fluid Mech.* **234**, 19–46.

DANGELMAYR, G. 1986 Steady-state mode interaction in the presence of $O(2)$ symmetry. *Dyn. Stab. Syst.* **1**, 159–185.

DANGELMAYR, G. & KNOBLOCH, E. 1987 The Takens–Bogdanov bifurcation with $O(2)$ symmetry. *Phil. Trans. R. Soc.* A **322**, 243–279.

DEARDORFF, J. W. & WILLIS, G. E. 1965 The effect of two-dimensionality on the suppression of thermal turbulence. *J. Fluid Mech.* **23**, 337–353.

DRAKE, J. F., FINN, J. M., GUZDAR, P. N., SHAPIRO, V., SHEVCHENKO, V., WAELBROECK, F., HASSAM, A. B., LIU, C. S. & SAGDEEV, R. 1992 Peeling of convection cells and the generation of sheared flow. *Phys. Fluids* B **4**, 488–491.

FINN, J. M. 1993 Nonlinear interaction of Rayleigh–Taylor and shear instabilities. *Phys. Fluids* B **5**, 413–432.

FINN, J. M., DRAKE, J. F. & GUZDAR, P. N. 1992 Instability of vortices and generation of sheared flow. *Phys. Fluids* B **4**, 2758–2768.

GINET, G. P. & SUDAN, R. N. 1987 Numerical observations of dynamic behavior in two-dimensional compressible convection. *Phys. Fluids* **30**, 1667–1677.

GRAHAM, E. 1975 Numerical simulation of two-dimensional compressible convection. *J. Fluid Mech.* **70**, 689–703.

GROSSMANN-DOERTH, U., KNÖLKER, M., SCHÜSSLER, M. & SOLANKI, S. K. 1994 The deep layers of solar magnetic elements. *Astron. Astrophys.* **285**, 648–654.

GUCKENHEIMER, J. & HOLMES, P. 1983 *Nonlinear Oscillations, Dynamical Systems and Bifurcations of Vector Fields*. Springer.

HOWARD, L. N. & KRISHNAMURTI, R. 1986 Large-scale flow in turbulent convection: a mathematical model. *J. Fluid Mech.* **170**, 385–410.

HUGHES, D. W. & PROCTOR, M. R. E. 1988 Magnetic fields in the solar convection zone: magnetoconvection and magnetic buoyancy. *Ann. Rev. Fluid Mech.* **20**, 187–223.

HUGHES, D. W. & PROCTOR, M. R. E. 1990 A lower order model for the shear instability of convection, chaos and the effect of noise. *Nonlinearity* **3**, 127–153.

HURLBURT, N. E., PROCTOR, M. R. E., WEISS, N. O. & BROWNJOHN, D. P. 1989 Nonlinear compressible magnetoconvection. Part 1. Travelling waves and oscillations. *J. Fluid Mech.* **207**, 587–628.

HURLBURT, N. E. & TOOMRE, J. 1988 Magnetic fields interacting with nonlinear compressible convection. *Astrophys. J.* **327**, 920–932.

HURLBURT, N. E., TOOMRE, J. & MASSAGUER, J. M. 1984 Two-dimensional compressible convection extending over multiple scale heights. *Astrophys. J.* **282**, 557–573.

JONES, C. A. & PROCTOR, M. R. E. 1987 Strong spatial resonance and travelling waves in Bénard convection. *Phys. Lett.* A **21**, 224–227.

JULIEN, K. 1991 Strong spatial resonance in convection. PhD dissertation, University of Cambridge.

JULIEN, K., BRUMMELL, N. & HART, J. E. 1993 Travelling waves in convection with large-scale flows. Preprint.

KNOBLOCH, E. & PROCTOR, M. R. E. 1981 Nonlinear periodic convection in double-diffusive systems. *J. Fluid Mech.* **108**, 291–316.

KNOBLOCH, E., PROCTOR, M. R. E. & WEISS, N. O. 1992 Heteroclinic bifurcations in a simple model of double-diffusive convection. *J. Fluid Mech.* **239**, 273–292.

KNOBLOCH, E., WEISS, N. O. & DA COSTA, L. N. 1981 Oscillatory and steady convection in a magnetic field. *J. Fluid Mech.* **113**, 153–186.

KRISHNAMURTI, R. & HOWARD, L. N. 1981 Large-scale flow generation in turbulent convection. *Proc. Natl Acad. Sci.* **78**, 1981–1985.

LANDSBERG, A. S. & KNOBLOCH, E. 1991 Direction-reversing traveling waves. *Phys. Lett.* A **159**, 17–20.

LANTZ, S. R. 1994 Magnetoconvection dynamics in a stratified layer. II. A low-order model of the tilting instability. *Astrophys. J.* (in press).

LANTZ, S. R. & SUDAN, R. N. 1994 Magnetoconvection dynamics in a stratified layer. I. 2D simulations and visualization. *Astrophys. J.* (in press).

MATTHEWS, P. C. 1993 Compressible magnetoconvection in three dimensions. In *Theory of Solar and Planetary Dynamos* (ed. M. R. E. Proctor, P. C. Matthews & A. M. Rucklidge), pp. 211–218. Cambridge University Press.

MATTHEWS, P. C., PROCTOR, M. R. E., RUCKLIDGE, A. M. & WEISS, N. O. 1993 Pulsating waves in nonlinear magnetoconvection. *Phys. Lett.* A **183**, 69–75.

MATTHEWS, P. C., PROCTOR, M. R. E., RUCKLIDGE, A. M. & WEISS, N. O. 1994*a* Pulsating waves in two- and three-dimensional magnetoconvection. In preparation.

MATTHEWS, P. C., PROCTOR, M. R. E. & WEISS, N. O. 1994*b* Compressible magnetoconvection in three dimensions: planform selection and weakly nonlinear behaviour. *J. Fluid Mech.* (submitted).

MOORE, D. R. & WEISS, N. O. 1990 Dynamics of double convection. *Phil. Trans. R. Soc. Lond.* A **332**, 121–134.

NORDLUND, Å. & STEIN, R. F. 1990 Solar magnetoconvection. In *Solar photosphere: structure, convection and magnetic fields* (ed. J. O. Stenflo), pp. 191–211. Kluwer.

PRAT, J., MASSAGUER, J. M. & MERCADER, I. 1993 Mean flow in 2D thermal convection. In *Mixing in geophysical flow* (ed. J. M. Redondo & O. Metais). Barcelona: Diseño Gráfico.

PROCTOR, M. R. E. 1986 Columnar convection in double-diffusive systems. *Contemp. Maths* **56**, 267–276.

PROCTOR, M. R. E. 1992 Magnetoconvection. In *Theory and Observation of Sunspots* (ed. J. H. Thomas & N. O. Weiss), pp. 221–241. Kluwer.

PROCTOR, M. R. E. & JONES, C. A. 1988 The interaction of two spatially resonant patterns in thermal convection. Part 1. Exact 1:2 resonance. *J. Fluid Mech.* **188**, 301–335.

PROCTOR, M. R. E. & WEISS, N. O. 1982 Magnetoconvection. *Rep. Prog. Phys.* **45**, 1317–1379.

PROCTOR, M. R. E. & WEISS, N. O. 1990 Normal forms and chaos in thermosolutal convection. *Nonlinearity* **3**, 619–637.

PROCTOR, M. R. E. & WEISS, N. O. 1993 Symmetries of time-dependent magnetoconvection. *Geophys. Astrophys. Fluid Dyn.* **70**, 137–160.

RUCKLIDGE, A. M. & MATTHEWS, P. C. 1993 Shearing instabilities in magnetoconvection. In *Theory of Solar and Planetary Dynamos* (ed. M. R. E. Proctor, P. C. Matthews & A. M. Rucklidge), pp. 257–264. Cambridge University Press (referred to herein as RM).

RUCKLIDGE, A. M. & MATTHEWS, P. C. 1994 Analysis of the shearing instability in nonlinear magnetoconvection. In preparation (referred to herein as RM).

SCHNAUBELT, M. & BUSSE, F. H. 1992 Convection in a rotating cylindrical annulus. Part 3. Vacillating and spatially modulated flows. *J. Fluid Mech.* **245**, 155–173.

THOMAS, J. H. & WEISS, N. O. 1992 The theory of sunspots. In *Theory and Observation of Sunspots* (ed. J. H. Thomas & N. O. Weiss), pp. 3–59. Kluwer.

WEISS, N. O. 1981 Convection in an imposed magnetic field. Part 1. The development of nonlinear convection. *J. Fluid Mech.* **108**, 247–272.

WEISS, N. O. 1989 Time-dependent compressible magnetoconvection. In *Solar and Stellar Granulation* (ed. R. J. Rutten & G. Severino), pp. 471–480. Kluwer.

WEISS, N. O. 1991 Magnetoconvection. *Geophys. Astrophys. Fluid Dyn.* **62**, 229–247.

WEISS, N. O., BROWNJOHN, D. P., HURLBURT, N. E. & PROCTOR, M. R. E. 1990 Oscillatory convection in sunspot umbrae. *Mon. Not. R. Astron. Soc.* **245**, 434–452.